Numerical simulation of particle segregation in a bidisperse suspension

Raphael Pesche, Georges Bossis, Alain Meunier

NUMERICAL SIMULATION OF PARTICLE SEGREGATION IN A BIDISPERSE SUSPENSION

Raphaël PESCHE
Fakultät für Physik, Universität Konstanz, Postfach 5560, D-78457 Konstanz, Germany

Georges BOSSIS and Alain MEUNIER
Laboratoire de Physique de la matière condensée, CNRS UMR 6622, Université de Nice-Sophia-Antipolis, 06108 Nice Cedex 2, France

Key words: shear-induced migration, bidisperse suspension, cylindrical Couette flow, simple shear flow, hydrodynamic interactions.

Abstract: We have performed numerical simulations of a monolayer of a bidisperse suspension of colloidal particles in a cylindrical Couette flow taking into account hydrodynamic interactions (HI). We compare our simulation results with a simple phenomenological model and obtain good agreement for the monodisperse case. For a bidisperse suspension, we also obtain a good agreement if the ratio of the radii of the two kind of particles is smaller than 0.5. In a second part, we simulate a two-dimensional bidisperse suspension submitted to a simple shear flow and observe, when HI are disregarded, a local segregation with the formation of stripes along the velocity lines.

1. Introduction

An important amount of experimental studies deals with the influence of the shear rate on the concentration profile of monodisperse particle suspensions. One generally observe a migration to the region of lower shear rate Karnis et al. (1966), Arp and Mason (1977), Gadala-Maria and Acrivos (1980), Leighton and Acrivos (1987), Abbott et al. (1991). This phenomenon exists even for vanishingly small Reynolds number and inertia forces can be neglected for Re_p smaller than 0.01 ,Han and Kim (1999). Some mechanisms have been

proposed to explain the migration directed along the flow velocity gradient. Thanks to technics not perturbative for the system (nuclear magnetic resonance (NMR) and laser Doppler anemometry), it is now possible to measure the density and the velocity profiles in dense suspensions.

The model proposed by Leighton and Acrivos (1987) takes into account the spatial variation of both the frequency of collisions between the suspended particles and the effective viscosity. Using NMR, Abbot et al. (1991), observed, in a cylindrical Couette flow, a particle volume flux proportional to the shear rate and $a^{2.6}$, where a is the particle radius. The power dependency with the particles radius is not exactly the a^2 dependency found by Leighton and Acrivos (1987) using dimensional arguments.

It is clear that the migration phenomenon can't be predicted by the Stokes equations alone. These equations predict a symetric trajectory along the velocity gradient for two hydrodynamically interacting particles.On the contrary, the presence of non hydrodynamics interactions (magnetic forces, electrostatic forces, contact forces) breaks the reversibility of the trajectories and induces some random motion which will give rise to migration mechanisms.. With the help of the ideas of Leighton and Acrivos (1987), Philips & al. (1992), have developped a constitutive equation for the particles flux. This one dimension model predicts a migration of the particles towards the outer wall (where the shear rate is minimum) and gives a satisfying agreement with the experimental concentration profile. In an axially symetric Poiseuille flow, this model predicts a migration towards the axis of the tube, with the onset of a blunted velocity profile which is similar to the well known "plug flow" observed in cylindrical Poiseuille flows. For bidisperse suspensions the results are scarce: it has been observed by D.M.Husband et al (1994) that coarse particles go outwards in a cylindrical Couette cell and some measurements of the tracer shear induced diffusion in bidisperse suspension have been carried out by Krishnan et al (1996), but we are not aware of a detailed experimental study of the migration mechanisms in a bidisperse suspension. The

aim of this paper is to use Stokesian dynamic simulation in order to study the migration mechanisms in sheared bidisperse suspension. The generalization of the model of Philipps & al to bidisperse suspension was developped in order to compare with the numerical results obtained by Stokesian dynamics,R.Pesché (1998), R.Pesché &al (1998). A similar approach was developped independently by Shauly &al (1998)at the same timethis model and we shto model(and togeneralize the model of Philipps et al to this case .

Several methods may be used to perform numerical simulations of suspensions. A global approach based on a description involving constitutive equations has been done by Fang and Phan-Thien (1995) with a finite volume method. The main advantage is the small memory amount required and rather quick computational times. It is therefore possible to simulate complex systems using a simple workstation. Fang and Phan-Thien have used the phenomenological equation of Philips et al. (1992) for two dimensional flows with various geometries. In particular, in an excentred circular geometry, it appears a migration towards the external cylinder.This approach could be used for bidisperse suspensions if we know the equations which describe the evolution of the volume fraction of each species.The derivation of this system of equation is one of the goals of this paper, the other goal being to use a Stokesian dynamics simulation in a Couette flow in order to provide data which can be used to check the validity of these models.

Our paper is divided in to main parts. First, with the help of a Stokesian Dynamic numerical method (Durlofsky et al. (1987), Bossis and Brady (1992)), we simulate a suspension of colloidal particles in a cylindrical Couette flow geometry. In this part, we introduce the formalism and the numerical method we used to simulate a suspension of bidisperse particles. We also adopt a phenomenological point of vue of the diffusive mechanisms that induce a shear induced migration (and even a size segregation) in the suspension. We then compare the two approaches (phenomenological and numerical). In the second part, we present a

numerical simulation of a two-dimensional bidisperse system undergoing a simple shear flow and assess the importance of the hydrodynamic interaction (HI).

In this whole work, we consider suspensions of non brownian particles.

2. Shear-induced migration in a cylindrical Couette flow

2.1 Simulation method

Let us consider N suspended particles. Under the influence of an imposed velocity field, the particles move and interact indirectly through the suspending fluid. The linearity of Stokes equations allows to relate the translationnal and angular velocities of the particles to the forces and torques acting on each particle. This can be expressed as, Brenner and O´Neill (1972):

$$\delta\mathbf{U} = \mathbf{U} - \mathbf{U}^{\infty} = \mathbf{R}_{FU}^{-1}[\mathbf{F}^{nh} + \mathbf{R}_{FE} : \mathbf{E}^{\infty}] \ , \qquad (1)$$

where $\mathbf{U}^{\infty}$ is the imposed fluid velocity without the presence of the particles; $\mathbf{U} - \mathbf{U}^{\infty}$ being the perturbation velocity due to the presence of the particles. Note that these 6N vectors contain both the translational and rotational velocities. The matrix $\mathbf{R}_{FE}$ links the hydrodynamic forces to the symmetric part of the velocity gradient tensor, $\mathbf{E}^{\infty}$:

$$E_{ij}^{\infty} = \frac{1}{2}\left(\frac{\partial U_i^{\infty}}{\partial x_j} + \frac{\partial U_j^{\infty}}{\partial x_i} \right) \qquad (2)$$

The resistance matrix $\mathbf{R}_{FU}$ links the force-torque vector to the velocity vector. The $\mathbf{R}_{FU}$ and $\mathbf{R}_{FE}$ matrices depend only on the instantaneous configuration of the particles Happel and

Brenner (1965). Their analytical expression is given by Jeffrey and Onishi (1984), Kim and Mifflin (1985), Jeffrey (1992). $\mathbf{F}^{nh}$ is a pairwise additive non hydrodynamic colloidal force. We took a Debye-Huckel force in the linear Derjaguin approximation:

$$F^{nh} = f\frac{e^{-\tau\varepsilon}}{1-e^{-\tau\varepsilon}} \ , \qquad (3)$$

where ε is the surface separation berween two spheres. We follow Brady et al. (1985) and take $\tau / a = 227$ where a is the particle radius. The parameter f is chosen in such a way that $F^{nh}(\varepsilon / a = 0.01)$ is of the order of the hydrodynamic force.

Since we are interested in radial migration, we simulate one layer of fluid perpendicular to the cylinders axis. As a consequence, each particle has only two translational degrees of freedom and one for rotation. The computational cost will be strongly reduced.

We compute the hydrodynamic interactions only in a 60° angular area (fig. 1). The other part of the system is taken into account with $\pm 60°$ rotations from the central angular sector. Let N be the number of particles in this angular sector. The two neighbouring sectors contain each N image-particles. Let us writting the link between the force-torque vector of the 3N particules (central angular sector and the two neighbouring sectors) and the respective velocity perturbations:

$$\begin{pmatrix} \mathbf{F}_0 \\ \mathbf{F}_> \\ \mathbf{F}_< \\ \mathbf{T}_0 \\ \mathbf{T}_> \\ \mathbf{T}_< \end{pmatrix} = \begin{pmatrix} \mathbf{R}_{F_0\_V_0} & \mathbf{R}_{F_0\_V_>} & \mathbf{R}_{F_0\_V_<} & \mathbf{R}_{F_0\_\Omega_0} & \mathbf{R}_{F_0\_\Omega_>} & \mathbf{R}_{F_0\_\Omega_<} \\ \mathbf{R}_{F_>\_V_0} & \mathbf{R}_{F_>\_V_>} & \mathbf{R}_{F_>\_V_<} & \mathbf{R}_{F_>\_\Omega_0} & \mathbf{R}_{F_>\_\Omega_>} & \mathbf{R}_{F_>\_\Omega_<} \\ \mathbf{R}_{F_<\_V_0} & \mathbf{R}_{F_<\_V_>} & \mathbf{R}_{F_<\_V_<} & \mathbf{R}_{F_<\_\Omega_0} & \mathbf{R}_{F_<\_\Omega_>} & \mathbf{R}_{F_<\_\Omega_<} \\ \mathbf{R}_{T_0\_V_0} & \mathbf{R}_{T_0\_V_>} & \mathbf{R}_{T_0\_V_<} & \mathbf{R}_{T_0-\Omega_0} & \mathbf{R}_{T_0\_\Omega_>} & \mathbf{R}_{T_0\_\Omega_<} \\ \mathbf{R}_{T_>\_V_0} & \mathbf{R}_{T_>\_V_>} & \mathbf{R}_{T_>\_V_<} & \mathbf{R}_{T_>-\Omega_0} & \mathbf{R}_{T_>\_\Omega_>} & \mathbf{R}_{T_>\_\Omega_<} \\ \mathbf{R}_{T_<\_V_0} & \mathbf{R}_{T_<\_V_>} & \mathbf{R}_{T_<\_V_<} & \mathbf{R}_{T_<-\Omega_0} & \mathbf{R}_{T_<\_\Omega_>} & \mathbf{R}_{T_<\_\Omega_<} \end{pmatrix} \begin{pmatrix} \delta\mathbf{V}_0 \\ \delta\mathbf{V}_> \\ \delta\mathbf{V}_< \\ \delta\mathbf{\Omega}_0 \\ \delta\mathbf{\Omega}_> \\ \delta\mathbf{\Omega}_< \end{pmatrix} \qquad (4)$$

Here, $\mathbf{F}_0$ is the force vector (containing the hydrodynamic and non-hydrodynamic parts) applied to the particles in the central sector, $\mathbf{F}_>$ and $\mathbf{F}_<$ are its equivalent for the sector obtained by a +60° and -60° rotation respectively. $\mathbf{T}_0$ is the torque vector applied to the particles that belong to the central sector etc... The vectors $\delta\mathbf{V}_{0,>,<}$ and $\delta\boldsymbol{\Omega}_{0,>,<}$ are related to the translational velocity and angular velocity perturbations respectively. For example, the 2Nx2N submatrix $\mathbf{R}_{F_0-V_0}$ is the resistance matrix that links the forces and velocities of the particles located in the central sector. We can notice that the torque and the angular velocity perturbation applied to a particle is identical to the torque and angular velocity applied to its image.

$$\mathbf{T}_0 = \mathbf{T}_> = \mathbf{T}_<; \qquad \delta\boldsymbol{\Omega}_0 = \delta\boldsymbol{\Omega}_> = \delta\boldsymbol{\Omega}_< \qquad (5)$$

It is possible to write in a simply way a resistance matrix relative to the N particles located in the central box considering that each of them is in interaction with N-1 particles located in a 60° angular sector around it (fig. 1). From (3), and taking into account that the force vectors and velocities vectors of the image angular sectors are obtained from the central box by a $\pm 60°$ rotation, a straighforward calculation gives:

$$\begin{pmatrix} \delta\mathbf{V}_0 \\ \delta\boldsymbol{\Omega}_0 \end{pmatrix} = \mathbf{R}_{small}^{-1} \begin{pmatrix} \mathbf{F}_0 \\ \mathbf{T}_0 \end{pmatrix} \qquad (6)$$

with:

$$\mathbf{R}_{small}^{-1} = \begin{pmatrix} \mathbf{R}_{F_0\_V_0} + \mathbf{R}_{F_0\_V_>} : \Re_> + R_{F_0\_V_<} : \Re_< & \mathbf{R}_{F_0\_\Omega_0} + \mathbf{R}_{F_0\_\Omega_>} + \mathbf{R}_{F_0\_\Omega_<} \\ \mathbf{R}_{T_0\_V_0} + \mathbf{R}_{T_0\_V_>} : \Re_> + \mathbf{R}_{T_0\_V_<} : \Re_> & \mathbf{R}_{T_0\_\Omega_0} + \mathbf{R}_{T_0\_\Omega_>} + \mathbf{R}_{T_0\_\Omega_<} \end{pmatrix} \qquad (7)$$

where $\Re_>$ and $\Re_<$ are respectively +60° and -60° rotation matrices. The matrix $\mathbf{R}_{small}$ is then a 3Nx3N matrix.

As done in a previous work Pesche and Bossis (1999), we will only consider hydrodynamic interaction in the near field approximation. In this work, it has been shown that this simplification is justified in a shear flow.

To take into account the presence of the walls, we use the work by Bossis et al. 1991 that deals with the trajectory of a particle near a plan. We will suppose that a sphere coming close to a wall undergoes the influence of the plan tangential to this wall (fig. 2). Each couple sphere-wall will contribute to the building of the resistance matrix.

Let us briefly explain how we calculate the matrix $\mathbf{E}^{\infty}$ of Eq. (2). In a cylindrical Couette flow, the velocity at a distance r from the axis can be written

$$v_\theta = Pr + Q/r \ , \qquad (8)$$

Where P and Q depend on the velocities and sizes of the cylinders. We finally obtain, with the help of Eq. (2):

$$\mathbf{E}^{\infty} = \begin{pmatrix} -2\dfrac{\mathrm{Qyx}}{\mathrm{r}^4} & \dfrac{\mathrm{Q}}{\mathrm{r}^4}(\mathrm{x}^2-\mathrm{y}^2) & 0 \\ \dfrac{\mathrm{Q}}{\mathrm{r}^4}(\mathrm{x}^2-\mathrm{y}^2) & 2\dfrac{\mathrm{Qyx}}{\mathrm{r}^4} & 0 \\ 0 & 0 & 0 \end{pmatrix} \qquad (9)$$

with:

$$Q = \frac{(\Omega_1 - \Omega_2)R_1^2 R_2^2}{R_2^2 - R_1^2} \ , \qquad (10)$$

where Ω_1 and Ω_2 are the angular velocity of the inner and outer cylinder respectively. R_1 and R_2 are the radii of the inner and outer cylinders. In Eq. (9), x and y are the two-dimensional cartesian coordinates of the point where the shear matrix is evaluated. We have also $r^2 = x^2 + y^2$.

The radial dependency of the $\mathbf{E}^{\infty}$ tensor shows that the hydrodynamic forces will depend on the location of pair particles in the gap between the cylinders. For a given pair, we compute the shear matrix that corresponds to the center of the separating distance between the particles. This approximation is justified since the shear rate is nearly constant in the vicinity of two close spheres.

2.2 Phenomenological study

We generalise the work of Philips et al. (1991) for the bidisperse case. Let be Φ_b the volume fraction of the big specie and Φ_s the volume fraction of the small one. The corresponding particle radii are a_b and a_s.

2.2.1. Variable space interaction frequency

The particle volumic flux, J_c^{bb}, induced by pair collisions between big particles is obtained in the same way as Philips et al.:

$$J_c^{bb} = -K_c^b \Phi_b a_b^2 \nabla(\Phi_b \dot{\gamma}) \ , \quad (11)$$

where $\dot{\gamma}$ is the local shear rate. The coefficient K_c^b can be experimentaly evaluated. We suppose the case $a_b >> a_s$ and therefore consider that the motion of the big particles is not disturbed by the small ones:

$$J_c^{bs} \approx 0 . \qquad (12)$$

We have also for collisions between the small particles:

$$J_c^{ss} = -K_c^s \Phi_s a_s^2 \nabla(\Phi_s \dot{\gamma}) \qquad (13)$$

Now comes the problem of the small particles diffusion induced by the big ones. In the frame of a small particle, the rate of collisions with a big one is:

$$n_c^{sb} = \dot{\gamma} \rho_b \pi (a_s + a_b)^2 v_{sb} \qquad \text{with} \quad \lambda = \frac{a_s}{a_b} , \qquad (14)$$

where ρ_b is the number density of large particles and v_{sb} the relative velocity between the two particles. If we take $\dot{\gamma}(a_g + a_b)/2$ for its mean value:

$$v_{sb} = \frac{1}{a_s + a_b} \int_0^{a_s + a_b} \dot{\gamma} y dy =) \quad . \qquad (15)$$

Over a distance equal to the radius of a big particle, the difference in the collision number along the radial direction can be approximated as:

$$\Delta n_c^{sb} = \frac{dn_c^{sb}}{dy} a_b . \qquad (16)$$

Eventually, taking into account Eq. (13), we can write the total flux of small particles:

$$J_c^s = -K_c^s \Phi_s a_s^2 \nabla(\Phi_s \dot{\gamma}) - K_c^I \Phi_s a_b^2 \nabla(\Phi_b \dot{\gamma}), \qquad (17)$$

where $K_c^I = \frac{1}{8}(1+\lambda)^3(\lambda+\frac{1}{2})(\frac{2}{3}K_c^s)$.

2.2.2. Viscosity gradient

A non uniform distribution of particles induces a spatially dependence of the effective viscosity. The volumic flux of big particles induced by a gradient in the viscosity can be written:

$$J_\eta^{bb} = -K_\eta a_b^2 \dot{\gamma} \frac{\Phi_b^2}{\eta} \nabla \eta. \qquad (18)$$

In this section, we also suppose no modification of the trajectories of the big particles induced by the small ones. We will consider that the species are close enough to be in the lubrication range. Of course, we have:

$$J_\eta^{ss} = -K_\eta a_s^2 \dot{\gamma} \frac{\Phi_s^2}{\eta} \nabla \eta. \qquad (19)$$

Once again, we meet the difficulty to estimate the diffusion of the small particles induced by collisions with big ones. The hydrodynamic force component parallel to the velocity gradient which is exerced on the small particle is Kim and Karrila (1991):

$$F \approx \frac{12\pi a_s a_b \xi^{-1} \dot{\gamma}}{(1+\lambda)^3} \eta^i, \qquad (20)$$

where $\eta^i = \eta^+$ or η^- when the small particle pass over or under the other (fig. 3). ξ is the normalised surface separation:

$$\xi = \frac{r - a_s - a_b}{\frac{1}{2}(a_s + a_b)}. \qquad (21)$$

The small particle´s velocity is given by:

$$v_s \approx F / X_{sb}^A \quad \text{with ,,} \qquad (22)$$

where η is here an estimation of the mean viscosity. Eventually, we have:

$$v_s = \frac{a_b \dot{\gamma} \eta^i}{\eta}. \quad (23)$$

The displacement difference between the two trajectories (fig. 3) over a time interval $1/\dot{\gamma}$ is:

$$\Delta y = \Delta y^+ - \Delta y^- = \frac{a_b \eta^+}{\eta} - \frac{a_b \eta^-}{\eta} = \frac{a_b \Delta \eta}{\eta}. \qquad (24)$$

Where $\Delta\eta$ is the viscosity variation over a length a_b. We have then:

$$\Delta y = \frac{a_b^2 \nabla \eta}{\eta} \quad (25)$$

The corresponding flux is then:

$$J_\eta^{sb} = n_c^{sb} \Delta y \Phi_s \,. \qquad (26)$$

Using Eqs. (14) and (26), we get:

$$J_\eta^s = J_\eta^{sb} + J_\eta^{ss} = -K_\eta \dot{\gamma} \left(\frac{1}{8} \Phi_b (1+\lambda)^3 a_b^2 \Phi_s + a_s^2 \Phi_s^2 \right) \frac{\nabla \eta}{\eta} \,. \quad (27)$$

2.2.3. Curvature effect

In a curved geometry (flow between two parallel plates), Chow & al. (1994), have observed a new kind of flux. This is due to the fact that the direct colloidal force acting between a couple of particles has a radial outward component. For the fluxes corresponding to particles of the same specie, we follow Krishnan & al. (1996):

$$J_r^{bb} = K_r \dot{\gamma} \; a_b^2 \frac{\Phi_b^2}{r} \,, \quad (28a)$$

$$J_r^{ss} = K_r \dot{\gamma} \; a_s^2 \frac{\Phi_s^2}{r} \,. \quad (28b)$$

We are once again confronted with the interaction between a big and a small particle. We use the notations of Fig. 4. The radial velocity of particles 1 and 2 are given by:

$$v_1 = \frac{F_1 \cos(\phi - \theta)}{X_{sb}^A} \;\; ; \;\; v_2 = \frac{F_2 \cos(\phi + \theta)}{X_{sb}^A} . \qquad (29)$$

We suppose that $F_1 = F_2 = F_s$. The difference can be written:

$$\Delta v = v_1 - v_2 \cong \frac{2F_s < \sin(\phi) > \sin(\theta)}{X_{sb}^A} \cong \frac{2F_s < \sin(\phi) >}{X_{sb}^A} \frac{a_b + a_s}{r} . \qquad (30)$$

The repulsive force is of the order of the hydrodynamic force in the lubrication area. We then can suppose that $\frac{F_s}{X_{sb}^A} \approx \dot{\gamma} a_b$. Then comes the following expression for the small particle displacement:

$$\Delta y^{sb} \cong 2 \;\; a_b \frac{a_s + a_b}{r} , \qquad (31)$$

where we have supposed that the quantity $\frac{F_s}{X_{sb}^A}$ is of the order of $\dot{\gamma} a_g$. The small particle flux, with the participation of eq. (29b) can be written:

$$J_r^s = K_r \frac{\dot{\gamma}}{r} \left(\frac{1}{16} \Phi_b \Phi_s (1+\lambda)^3 a_b (a_s + a_b) + a_s^2 \Phi_s^2 \right) . \quad (32)$$

It seems reasonable to consider that the collisions happen with such a configuration that $\phi \approx \pi / 2$. We have therefore taken $< \sin(\phi) >= 1$.

At equilibrium, the small particles flux and the big particles flux vanish:

$$-\frac{K_c}{\Phi_b\dot{\gamma}}\nabla(\Phi_b\dot{\gamma})-\frac{K_\eta}{\eta}\nabla\eta+\frac{K_r}{r}=0 \qquad (33a)$$

$$-\frac{K_c}{\dot{\gamma}\Phi_s}\nabla(\Phi_s\dot{\gamma})-\frac{K_c}{\dot{\gamma}\Phi_s}m_1\nabla(\Phi_b\dot{\gamma})-K_\eta\left(1+m_2\frac{\Phi_b}{\Phi_s}\right)\frac{\nabla\eta}{\eta}+K_r\frac{1}{r}\left(1+m_3\frac{\Phi_b}{\Phi_s}\right)=0\,. \qquad (33b)$$

Eq. (33a) is obtained taking together (11), (18), (28a) and dividing the sum by $\Phi_b^2 a_b^2\dot{\gamma}$ for the big particles. For the other specie, eq. (33b) comes from (13), (17), (32) and dividing by $\Phi_s^2 a_s^2\dot{\gamma}$. We have also supposed that $K_c^s = K_c^b = K_c$. Indeed, we can suppose that the amplitude of the displacement of a particle, after a collision, in the direction perpendicular to the flow, is of the order of a particle's radius. We have also:

$$\mathrm{m}_1=\frac{1}{12}\frac{(1+\lambda)^3}{\lambda^2}\left(\frac{1}{2}+\lambda\right)\ ;\ \mathrm{m}_2=\frac{(1+\lambda)^3}{8\lambda^2};\quad \mathrm{m}_3=\frac{1}{16\lambda^2}(1+\lambda)^4 \qquad (34)$$

We have also taken into account the fact that in a cylindrical Couette flow:

$$\frac{1}{\dot{\gamma}}\frac{\mathrm{d}\dot{\gamma}}{\mathrm{dr}}=-\frac{1}{\eta}\frac{\mathrm{d}\eta}{\mathrm{dr}}-\frac{2}{\mathrm{r}} \qquad (35)$$

Now comes the question of the spatial dependance of the viscosity for a two species media. We consider the suspension as an effective media Quemada (1977), Van de Ven (1976):

$$\eta(\Phi,\ \Phi_s)=\left(1-\frac{\Phi-\Phi_s}{c_0}\right)^{\beta}\ , \qquad (36)$$

where $\Phi = \Phi_s + \Phi_b$ is the total particule concentration, c_0 is the maximal monodisperse compacity (≈ 0.68 for hard spheres). We follow Gondret (1994) and take $\beta = -3/2$. At last, eq. (33a) and (33b) become:

$$\left(\frac{3}{2}\frac{\Phi' - \Phi_b' c_1}{c_0 - \Phi + \Phi_b c_1} + \frac{1}{\Phi_b}\frac{2}{r} - \frac{1}{\Phi_b}\nabla(\Phi_b)\right) - K_\eta^* \frac{3}{2}\frac{\Phi' - \Phi_b' c_1}{c_0 - \Phi + \Phi_b c_1} + \frac{K_r^*}{r} = 0 \qquad (37a)$$

$$\left(\frac{3}{2}\frac{\Phi' - \Phi_b' c_1}{c_0 - \Phi + \Phi_b c_1} + \frac{1}{\Phi - \Phi_b}\frac{2}{r}\right) - \frac{1}{\Phi - \Phi_b}\nabla(\Phi - \Phi_b) + \frac{1}{\Phi - \Phi_b} m_1 \left(\Phi_b \left(\frac{3}{2}\frac{\Phi' - \Phi_b' c_1}{c_0 - \Phi + \Phi_b c_1} + \frac{2}{r}\right) - \nabla\Phi_b\right) - K_\eta^* \left(1 + m_2 \frac{\Phi_b}{\Phi - \Phi_b}\right)\frac{3}{2}\frac{\Phi' - \Phi_b' c_1}{c_0 - \Phi + \Phi_b c_1} + K_r^* \frac{1}{r}\left(1 + m_3 \frac{\Phi_b}{\Phi - \Phi_b}\right) = 0 \qquad (37b)$$

where $K_\eta^* = K_\eta / K_c$ and $K_r^* = K_r / K_c$.

2.3. Numerical simulation against phenomenological model

We have performed numerical simlations of systems containing 64 or 80 particles. We will present here four different radius ratios: $\lambda = \frac{a_s}{a_b}$=0.1, 0.2, 0.5, 1. In the monodisperse case ($\lambda = 1$), Fig. 5 shows the concentration profile for a system of 64 particles with mean volume fraction $\overline{\Phi} = 0.45$. This result was obtained after 100 laps of the inner cylinder, the outer one is still. At this time, the concetration profile remains constant. For every time step, the inner cylinder does a 5.10^{-3} radian rotation. This choice of the time step remains the same for the other following simulations in this section.The dashed line of Fig. 5a corresponds to the

solution of the equation of Philips et al. (1992) with a parameter $K_\eta^{*-1} = 0.75$. Note that this equation was obtained without taking into account the cuvature of the streamlines ($K_r^* = 0$). The full line is obtained with $K_\eta^{*-1} = 0.65$ and $K_\eta^{*-1} = 1$and allows to get a good agreement with the numerical points.

The figure 6a shows the concentrations profiles for a bidisperse suspension (40 big and 40 small) obtained by numerical simulation after 100 laps of the inner cylinder. The radius ration is $\lambda = 0.2$ and the mean concentrations $\overline{\Phi}_b = 0.45$ and $\overline{\Phi}_s = 0.02$. We have also reported the solution of (37a) and (37b) taking $K_\eta^{*-1} = 0.65$ and $K_r^* = 1$. We can see a picture of the half Couette flow with figure 6b. We observe a strong size segregation that is pretty good predicted by the phenomenological model. The big particles migrate toward the outer wall since they undergo greater deviations after collisions.

Figure 7 shows the concentrations profiles for a radius ratio $\lambda = 0.1$. Also in this case, the agreement between numerical and phenomenological studies is good. However it is bad with a radius ratio of 0.5 (figure 8). Indeed we have supposed that the motion of the big particles is not perturbed by the presence of the small ones. This approximation suffers when the radius ratio approaches $\lambda = 1$. We can see in Fig. 8 a size segregation obtained by numerical simulation that is not observed using the phenomenological model.

3. Phase separation under simple shear rate

Suspended particles interact each other with the colloidal repulsive force of Eq. (3). We present first results disregarding the HI. Each particles undergoes a Stokes drag force F^η as if it were alone in the fluid. At each time step, we have :

$$F^{nh} + F^{\eta} = 0 \ . \qquad (38)$$

The velocity of the particles is given by :

$$\mathbf{v} = \frac{\mathbf{F}^{rep}}{6\pi a \eta} + \dot{\gamma} y \hat{\mathbf{x}}, \qquad (39)$$

with a velocity in the x-direction due to the shear given by $\dot{\gamma} y$. The time step ised in the simulation is $\Delta t = 0.001\dot{\gamma}^{-1}$. Fig. 9 shows that the system becomes stripe structured. Santra et al. (1996) have obtained such a phase separation taking into account inertia of particles.

We have then performed numerical simulation of the same kind of system including HI. We proceed in the same way as in section 2.1. The difference is that in this case, the imposed shear rate is constant and the periodic boundary conditions are those usually used for a rectangular box. Because of the computational time increasing, we used a small number of particles. Fig. 10 allows to compare the effect of hydrodynamic interactions - that make little clusters of aggregating particles and prevents the stripes formation - with the case of a single repulsive force.

4. Conclusion

We have developed a numerical simulation including HI which allows to reproduce particle's migration in a monodisperse or a bidisperse suspension confined in a two dimensional Couette flow. The concentration profiles obtained by numerical simulation have been compared to the predictions of a phenomenological model. For a monodisperse suspension, we obtain a good agreement when we take into account the flux due to the curvature of the strealines. In the bidisperse case for a radius ratio $\lambda = 0.2$, we observe a strong segregation

with the large particles going towards the lower shear rate gradients. Our model for bidisperse suspensions fairly well predicts this behaviour without the addition of others parameters.

We assess the importance of HI in a two-dimensional colloidal suspension undergoing a simple shear rate. The HI avoid the formation of stripes observed in the simple case of particles interacting with a repulsive pairwise additive potential.

Acknowledgement

We thank the French company SNPE for his financial support, and the IDRIS center in France who provided the computer time.

References

Abbott, J.R., Tetlow, N., Graham, A.M., Altobelli, S.A., Fukushima, E., Mondy, L.A. and Stephens, T.S. 1991 Experimental observations of particle migration in concentrated suspensions : Couette flow, *J. Rheol.* **35** (5), 773-795.

Arp, P.A. and Mason, S.G. 1977 The kinetics of flowing dispersions. IX. Doublets of rigid spheres, *J. Colloidal Interface Sci.* **61**, 44-61.

Bossis, G. and Brady, J.F. 1992 Brownian and Stokesian Dynamics, *Macroscopic Simulations of Complex Hydrodynamic Phenomena, Plenum Press,* 255-269.

Bossis, G., Meunier, A. and Sherwood, J.D. 1991 Stokesian dynamics simulations of particle trajectories near a plane, *Phys. Fluids A* **3** (8), 1853-1858.

Brady, J. F. and Bossis, G. 1985 The rheology of concentrated suspensions of spheres in simple shear flow by numerical simulation, *J. Fluid Mech.* **195,** 105-129.

Brenner, H. and O'Neill, M. 1972 On the Stokes resistance of multiparticle systems in a linear shield filed, *Chem. Eng. Sc.*, **27**, 1421-1439.

Chow, A.W., Sinton, S.W., Iwamiya, J.H. and Stephens, T.S. 1994 Shear induced particle migration in Couette and parallel-plate viscometer : NMR imaging and stress measurements, *Phys. Fluids* **6** (8), 2561-2576.

Durlofsky, L., Brady, J.F. and Bossis, G. 1987 Dynamic simulation of hydrodynamically interacting particles, *J. Fluid Mech.* **180,** 21-49.

Fang, Z. and Phan-Thien, N. 1995 Numerical simulation of particle migration in concentrated suspensions by a finite volume method, *J. Non-Newtonian Fluid Mech.* **58,** 67-81.

Gadala-Maria, F. and Acrivos, A. 1980 Shear-induced structure in a concentrated suspensions of solid spheres, *J. Rheol.* **24** (6), 799-814.

Gondret, P. 1994 Hydrodynamique de suspensions monotailles et bitailles en écoulement oscillant, *PhD. thesis, Université Claude Bernard, Lyon-I.*

Han, M., Kim, C., Kim,M., Lee S. 1999 Particle migration in tube flow of suspensions J.Rheol. 43, 1157-1174

Happel, J. and Brenner, H. 1965 Low Reynolds number hydrodynamics, *Prentice Hall*.

Husband,D.M., Mondy,L.A.,Ganani, E. and Graham, A.L. (1994) Direct measurements of shear induced particle migrations, Rheologica Acta, **33**, 185-192

Jeffrey, D.J. 1992 The extended resistance functions for two unequal rigid spheres in low Reynolds number flow, *Phys. Fluids A* **4**, 16-29.

Jeffrey, D.J. and Onishi Y. 1984 Calculation of the resistance and mobility functions for two unequal rigid spheres in low Reynolds number flow, *J. Fluid Mech.* **139,** 261-290.

Karnis, A., Goldsmith, H.L. and Mason, S.G. 1966 The kinetic of flowing dispersions ; I : concentrated suspensions of rigid particles, *J. Colloid interface Sci.* **23**, 531.

Kim, S. and Mifflin, R.T. 1985 The resistance and mobility function of two equal spheres in low Reynolds number flow, *Phys. Fluids* **28**, 2033-2045.

Kim, S. and Karrila, S.J. 1991 Microhydrodynamics : Principles and selected applications, *Butterworth-Heinemann*.

Krishnan, G.P., Beimfohr, S. and Leighton, D.T. 1996 Shear-induced radial segregation in bidisperse suspensions, *J. Fluid Mech.* **321,** 371-393.

Leighton, D. and Acrivos, A. 1987 Measurement of shear-induced self-diffusion in concentrated suspensions of spheres, *J. Fluid Mech.* **177**, 109-131.

Pesche, R. and Bossis, G. 2000 The determination by stokesian dynamics of shear induced self diffusion coefficient in bidisperse suspensions, *submitted to J. Fluid Mech*.

Philips, R.J., Armstrong, R.C., Brown, R.A., Graham, A.L. and Abbott, J.R. 1992 A constitutive equation for concentrated suspensions that accounts for shear-induced particle migration, *Phys. Fluids A* **4** (1), 30-40.

Quemada, D. 1997 Rheology of concentrated disperse systems and minimum energy dissipation principle. I. Viscosity-concentration relationship, *Rheol. Acta* **16**, 82-74.

Santra, S.B., Schwarzer, S. and Herrmann, H. 1996 Fluid-induced particle-size segregation in sheared granular assemblies, *Phys. Rev. E,* **54**, 5066-5072.

Van de Ven, T.G. and Mason S.G. 1976 The microrheology of Colloidal Dispersions : IV. Pairs of Interacting spheres in Shear Flow, *J. Colloid interface Sci.* **57,** 3.

Figure captions

Figure 1: picture of the half Couette flow. The full circles represent the particles in the central angular area. The empty ones are their images. The full bright particle undergoes the influence of the nearest particles located in a 60° angular sector (delimited with dash lines) centered on it.

Figure 2: we consider that a particle (black circle) coming close to a wall interacts hydrodynamically with the plan tangential to this wall.

Figure 3: the small particle will undergo a more important displacement after collision since it will move in a media of weaker viscosity.

Figure 4: collision of two small particles with a big one. Particle 1 and 2 are ejected outward and inward respectively.

Figure 5: Results obtained for a monodisperse suspension with mean volume fraction $\overline{\Phi} = 0.45$. (a) concentration profile compared with theoretical prediction. The dashed line is obtained with $K_r^* = 0$ and $K_\eta^{*-1} = 0.75$; the full line with $K_r^* = 1$ and $K_\eta^{*-1} = 0.65$. (b) picture of the half Couette system.

Figure 6: $\lambda = 0.2$. (a) concentration profile for the two species.

Big particles, $\overline{\Phi}_b = 0.45$: • numerical simulation, — phenomenological model.

Small particles (x10), $\overline{\Phi}_s = 0.02$: ■ numerical simulation, --- phenomenological model.

(b) picture of the half Couette flow after 100 laps of the inner cylinder.

Figure 7: $\lambda = 0.1$. Concentration profile for the two species.

Big particles, $\overline{\Phi}_b = 0.45$: • numerical simulation, — phenomenological model.

Small particles x10, $\overline{\Phi}_s = 0.0045$: ■ numerical simulation, --- phenomenological model.

Figure 8: $\lambda = 0.5$. Concentration profile for the two species.

Big particles, $\overline{\Phi}_b = 0.41$: • numerical simulation, — phenomenological model.

Small particles $\overline{\Phi}_s = 0.1$: ■ numerical simulation, --- phenomenological model.

Figure 9: Two-dimensional suspension of 2000 particles (80 big and 1920 small) with mean concentration $\overline{\Phi}_b = 0.21$ and $\overline{\Phi}_s = 0.20$ at dimensionless time $T = 400\dot{\gamma}^{-1}$.

Figure 10: Two-dimensional suspension of 100 particles with mean concentration $\overline{\Phi}_b = 0.21$ and $\overline{\Phi}_s = 0.20$ at dimensionless time $T = 400\dot{\gamma}^{-1}$. (a) with HI; (b) with HI disregarded.

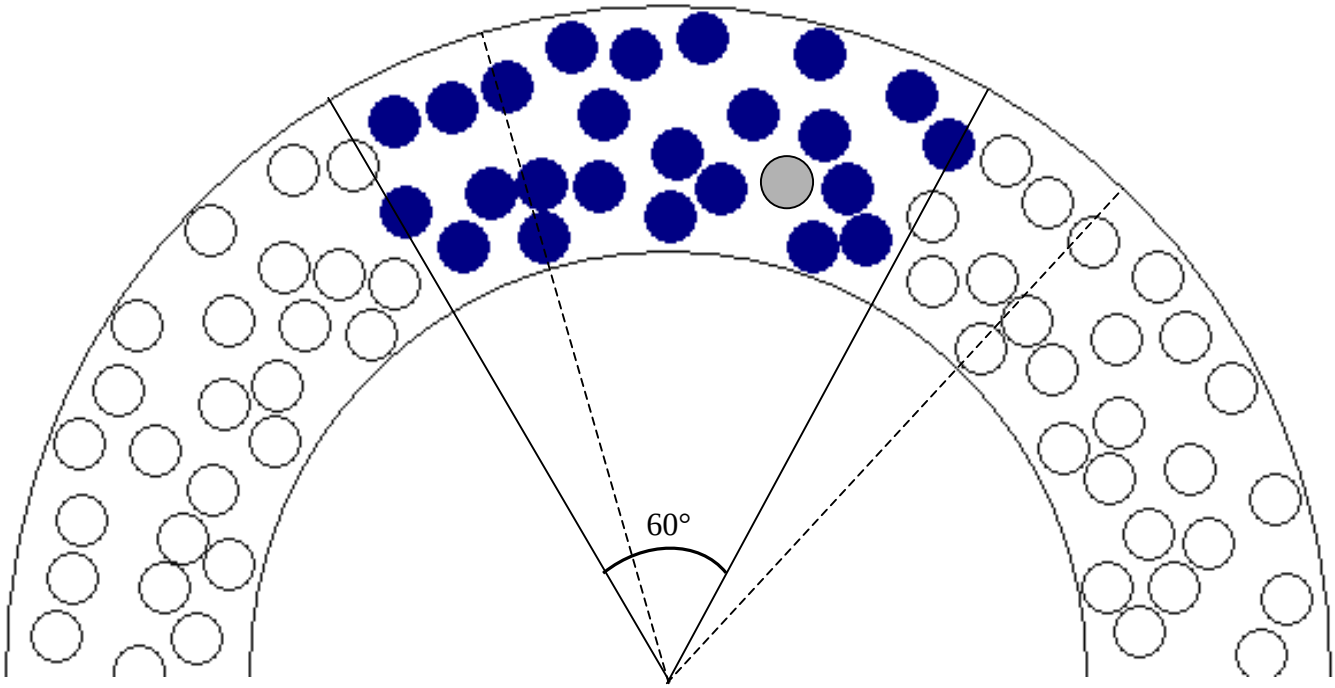

Figure 1

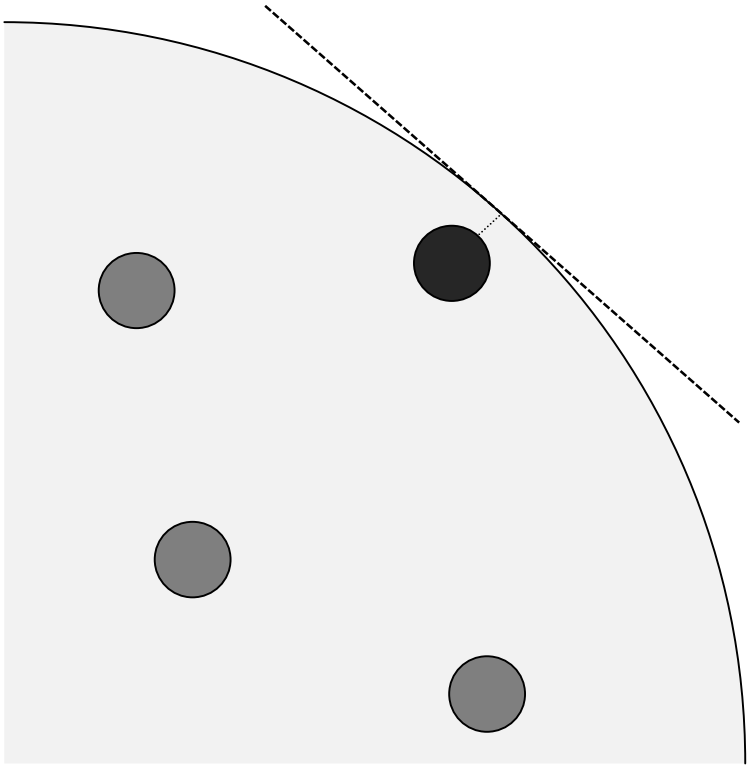

Figure 2

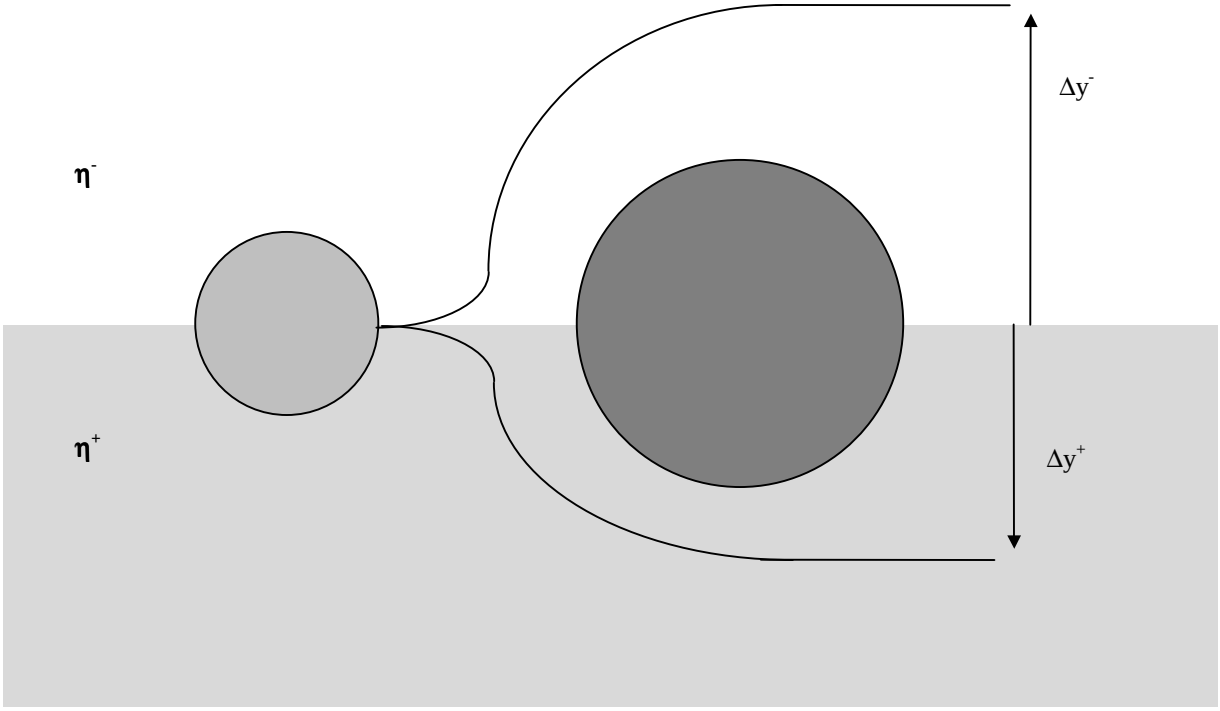

Figure 3

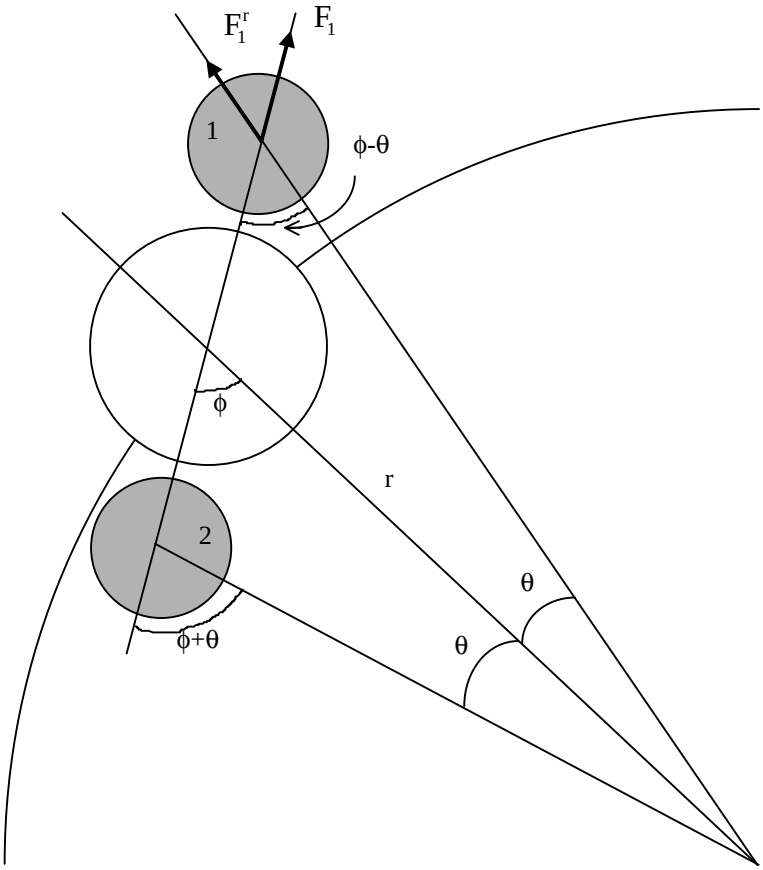

Figure 4

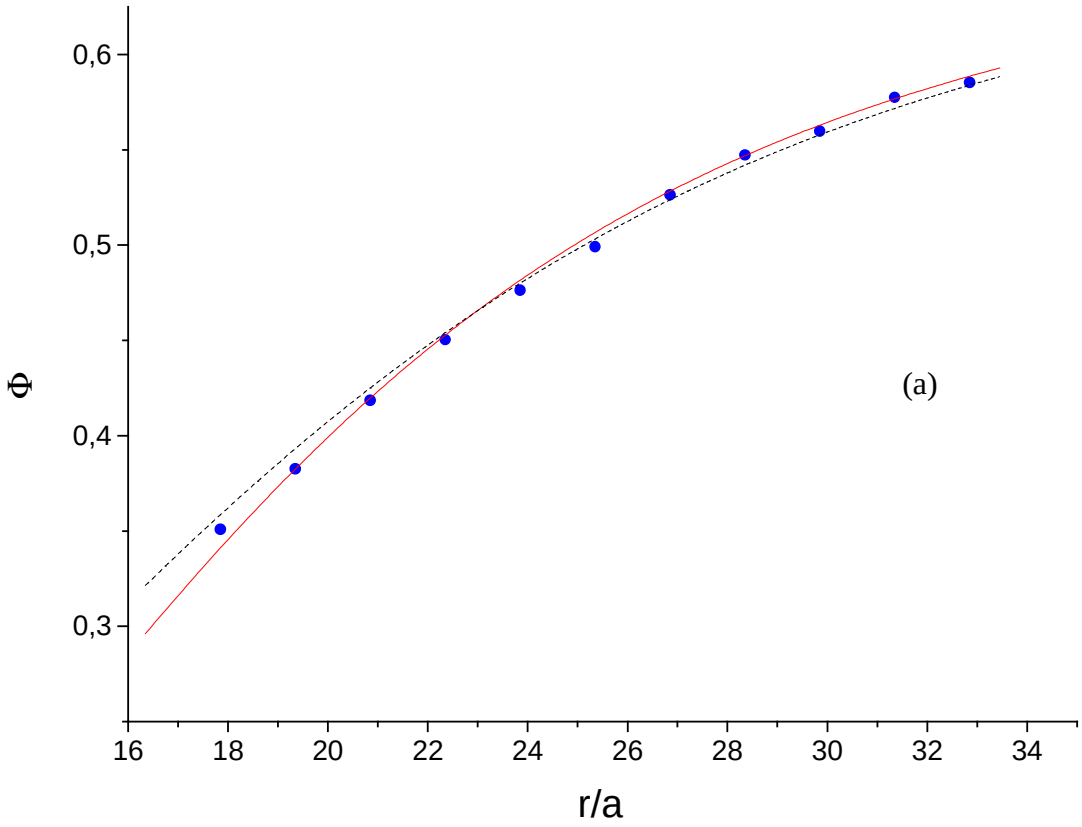

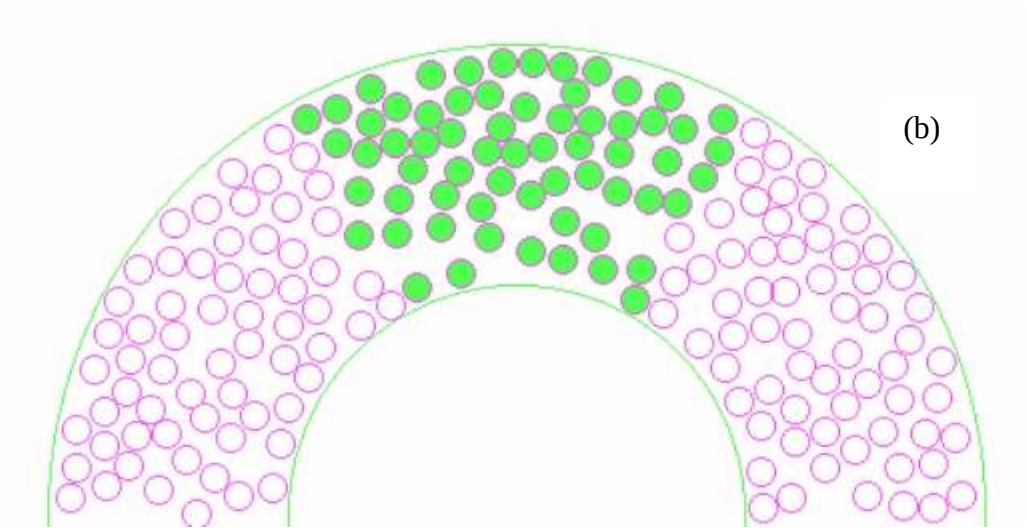

Figure 5.

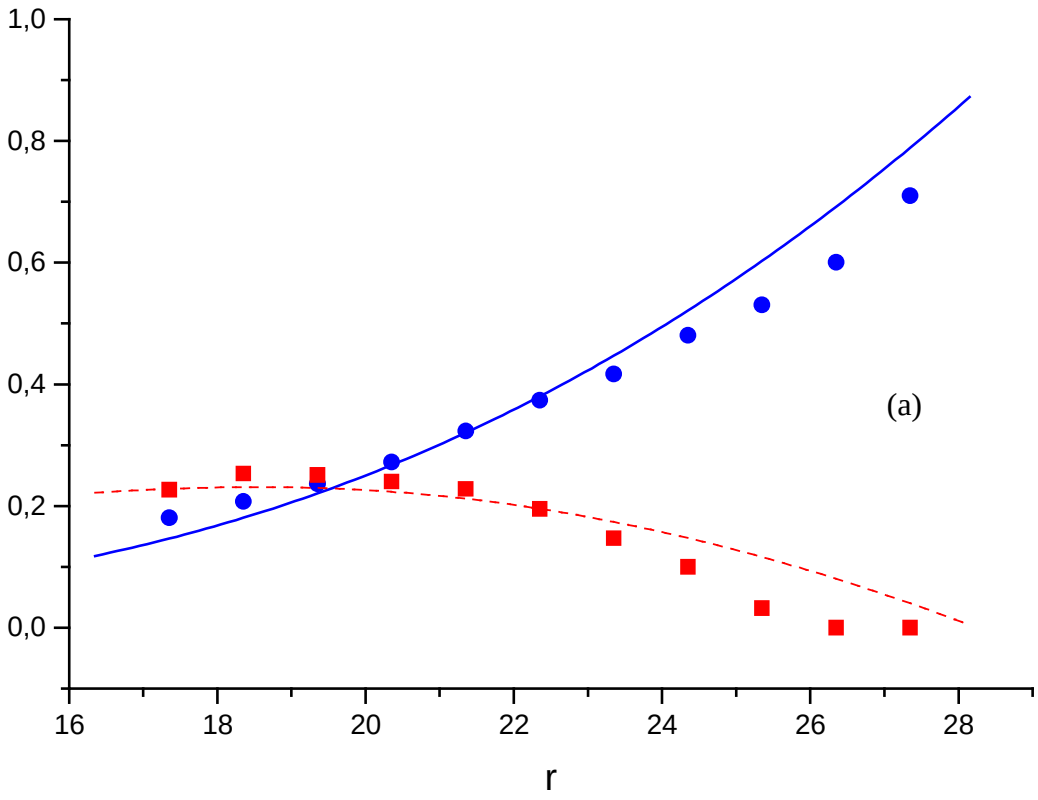

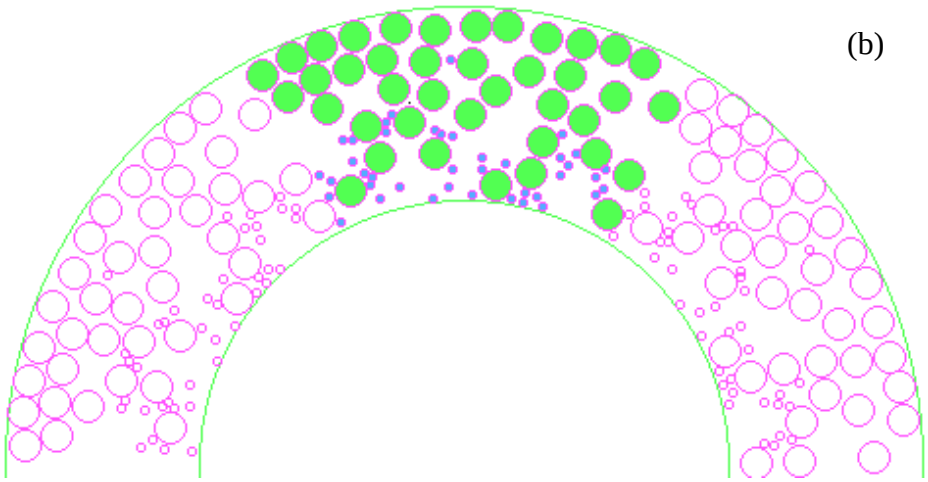

Figure 6

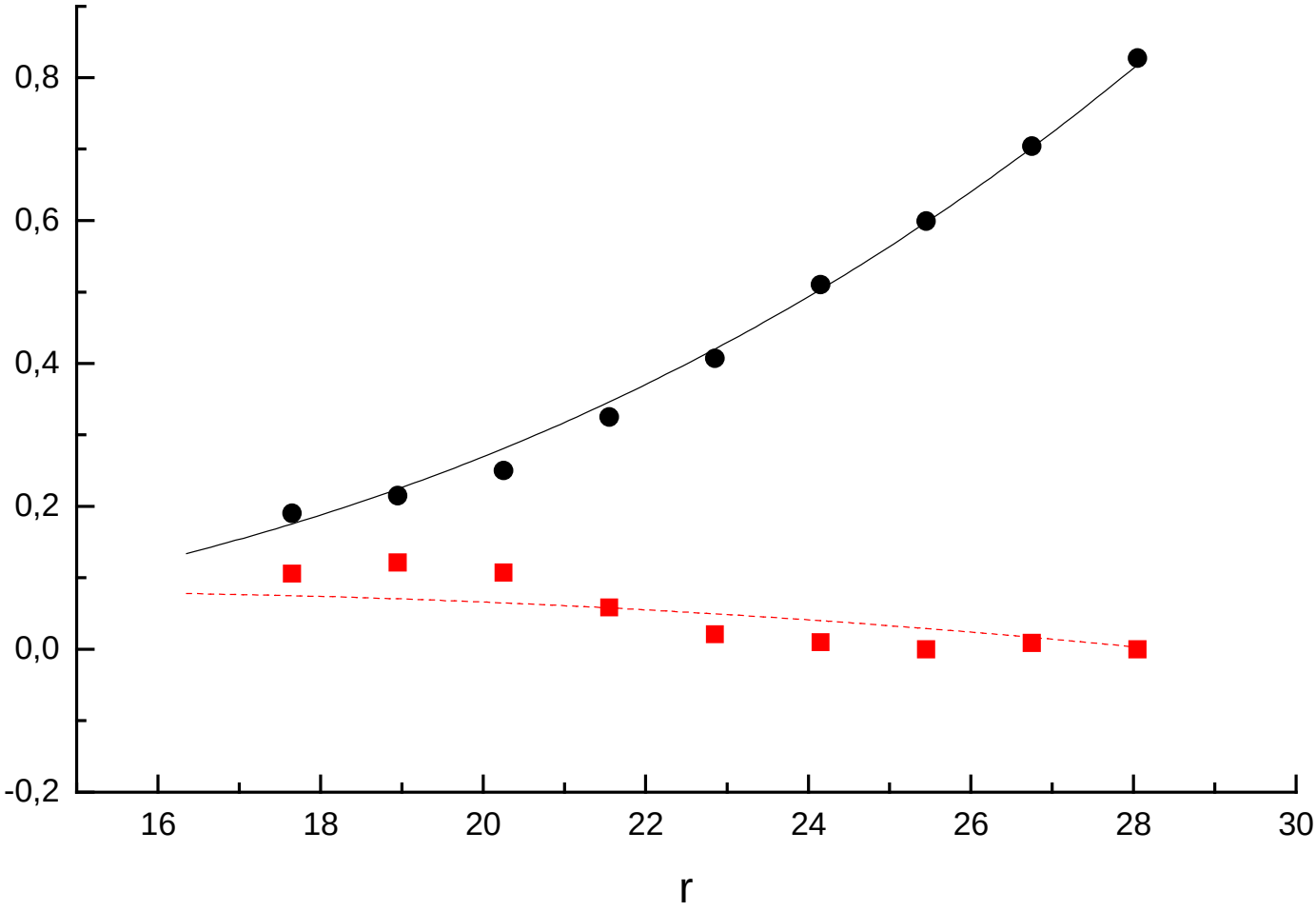

Figure 7

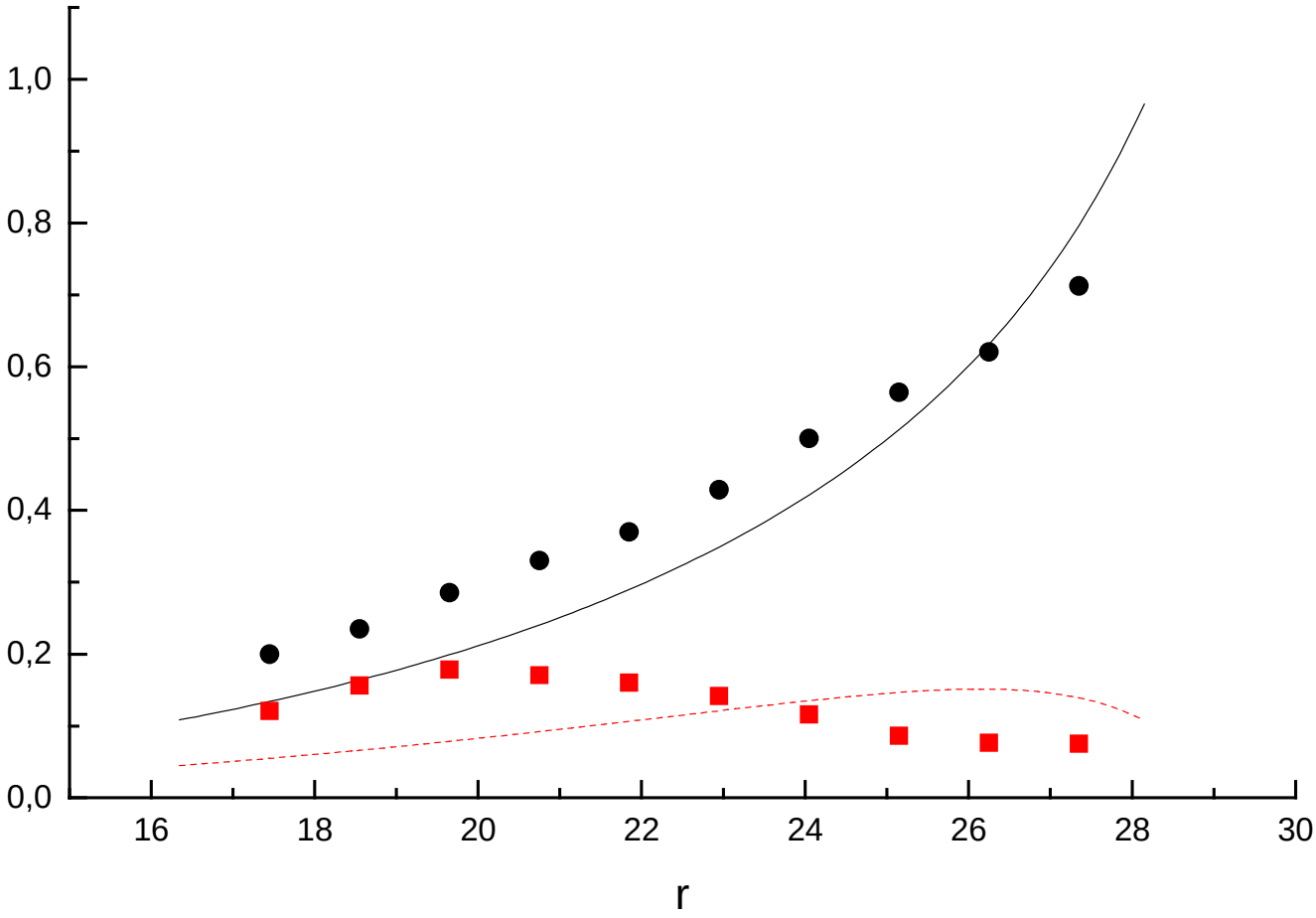

Figure 8

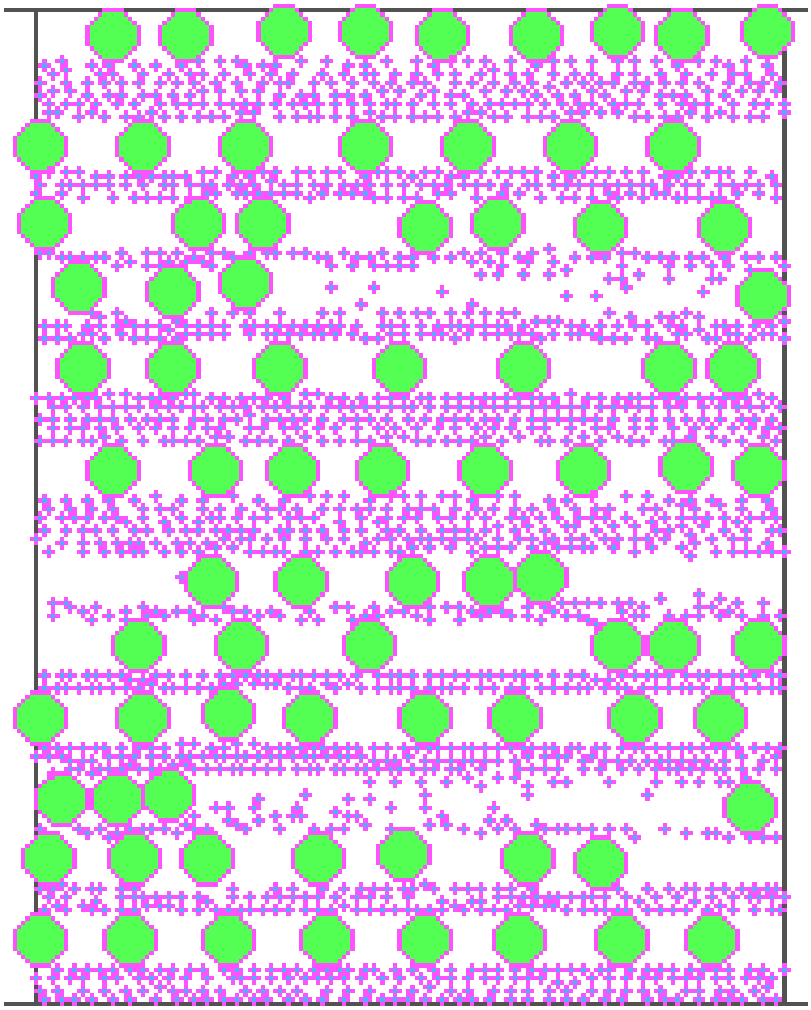

Figure 9

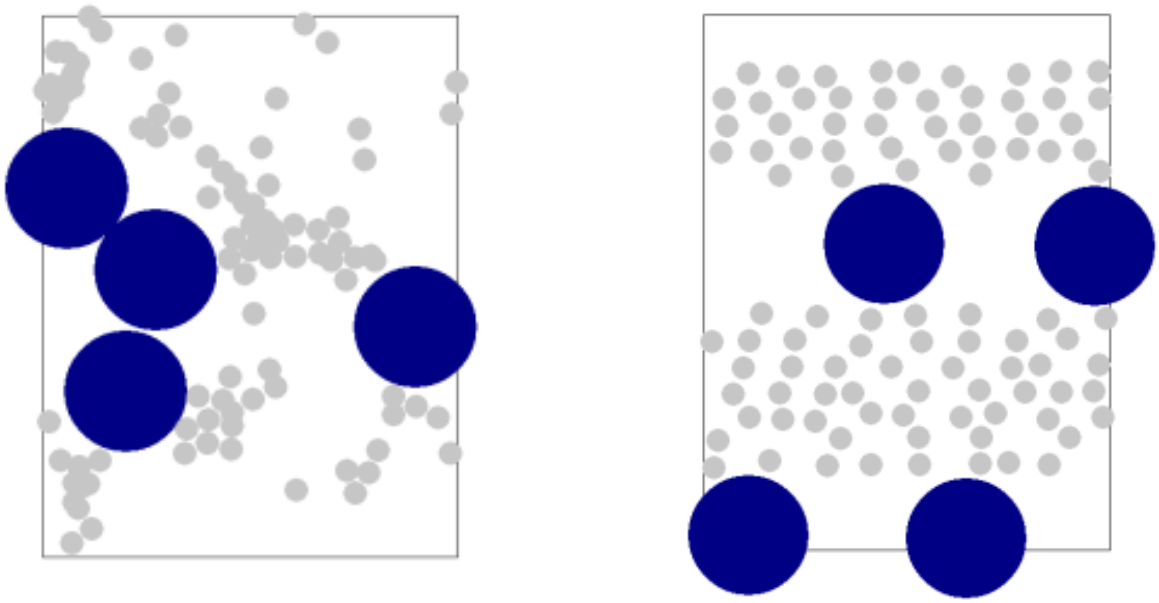

(a) (b)

Figure 10